JGR Biogeosciences

Key Points:
- Storm flow and external organic matter cause two thermoclines and 4-month long hypoxia
- Oxygen consumption and carbon dioxide emission are imbalanced in summer and winter
- Both the reservoir and downstream outflow are a net source of CO_2 to the atmosphere

Correspondence to:
N. Chen,
nwchen@xmu.edu.cn

Interaction Between Oxygen Consumption and Carbon Dioxide Emission in a Subtropical Hypoxic Reservoir, Southeastern China

Jing Yan[1], Nengwang Chen[1,2] , Fenfang Wang[1], Qian Liu[3], Zetao Wu[1], Jack J. Middelburg[4] , Yuyuan Xie[1,2] , Weidong Guo[1,2] , and Xin Zhang[5]

[1]Fujian Provincial Key Laboratory for Coastal Ecology and Environmental Studies, College of the Environment and Ecology, Xiamen University, Xiamen, China, [2]State Key Laboratory of Marine Environment Science, Xiamen University, Xiamen, China, [3]Key Laboratory of Marine Chemistry Theory and Technology, Ocean University of China, Qingdao, China, [4]Department of Earth Sciences, Utrecht University, Utrecht, The Netherlands, [5]Environmental Monitoring Centre of Fujian Province, Fuzhou, China

Abstract It is well recognized that dam construction aggravates eutrophication and hypoxia in river reservoirs, but the interaction between oxygen dynamics and carbon cycling is often unclear. Here we investigated the external and internal controls on oxygen consumption and effects of hypoxia on carbon dioxide (CO_2) emission in a subtropical reservoir in southeast China based on detailed field measurements during 2017 and 2018. Hypoxia lasted 4 months starting in mid-July and expanded from the bottom to near surface water. Rainstorm hyperpycnal flow and unusual hydraulics (outflow exit 40 m from the bottom) resulted in two thermoclines and enhanced the oxygen deficit in deeper water. Microbial respiration accounted for 67.4%–96.5% of total oxygen consumption in the bottom water. The increased supply of organic matter from storm runoff and to a lesser extent primary production in summer enhanced subsequent oxygen consumption. We observed an imbalance between excess CO_2 production and oxygen depletion in summer and winter which was likely associated with other processes in the hypolimnion (e.g., chemoautotrophy, anaerobic degradation of organic matter, proton buffering, and nitrification). The water-air CO_2 fluxes suggest that the surface reservoir usually served as a CO_2 source, but was a sink in summer due to high primary productivity. CO_2 was always oversaturated in the hypolimnion; this layer was at the depth of the dam outflow and ultimately released 68% of annual CO_2 efflux to the atmosphere. This research confirmed that construction of a hydropower dam has substantially altered reservoir metabolism and regulated the CO_2 emission pathway.

1. Introduction

Construction of dams in the channels of rivers form artificial reservoirs which change the transit time of water flowing from the catchment to the coast (Bednarek, 2001; Dynesius & Nilsson, 1994; Fearnside, 2001). Human activities in river basins (such as livestock and poultry production, and excessive application of chemical fertilizers) increase the discharge of dissolved nutrients and organic matter (OM) into the river channels, and consequently can cause eutrophication of downstream systems such as reservoirs (Bennett et al., 2001; Carpenter et al., 1998; Nearing et al., 2004; Smith et al., 1999). The construction of dams also alters the hydrological conditions within reservoirs including vertical stratification, which in turn profoundly modify the biogeochemical processes (oxygen, carbon, nitrogen, phosphorus, and silicon cycles) (Friedl & Wüest, 2002; Humborg et al., 2002; McClure et al., 2018) and alter the structure and function of aquatic communities (Rosenberg et al., 2000).

The interactive effects of increased eutrophication and thermal stratification on hypoxia has been recognized (Rabalais et al., 2010). Eutrophic, low-oxygen waters will also modify the production and emission of greenhouse gases (GHGs) such as carbon dioxide (CO_2), nitrous oxide (N_2O), and methane (CH_4), playing an important role in global carbon cycling and climate forcing (Moss et al., 2011; Tranvik et al., 2009). It has been reported that CO_2 emissions from reservoirs show high spatial-temporal variation and have large uncertainty (Deemer et al., 2016; Duchemin et al., 1995; Guerin et al., 2006; Huttunen et al., 2002; Kumar et al., 2019a; Li et al., 2018; Nowlin et al., 2004; Soumis et al., 2004; F. S. Wang et al., 2011). In addition, thermal stratification is well recognized as an important mechanism leading to hypoxia in both inland
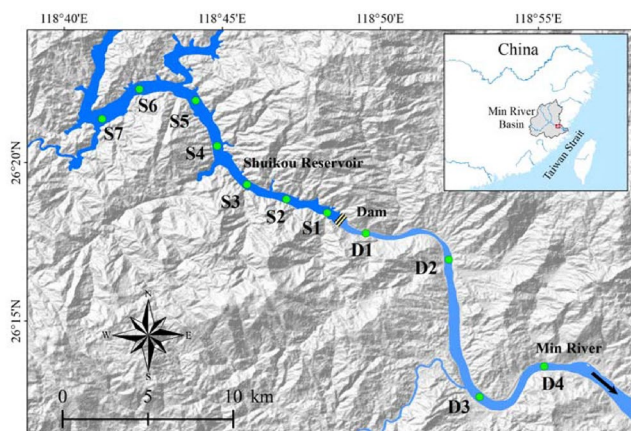
Figure 1. Map of the Shuikou reservoir and downstream river showing sampling sites.

waters and marine systems (MacIntyre et al., 2014; Prats et al., 2017; Yu et al., 2010). Compared to most lakes and the ocean, reservoirs are relatively sensitive to changes in hydrology of inflows (Nowlin et al., 2004). The thermal stratification structure in reservoirs is often affected by hyperpycnal flows (Long et al., 2016), which likely occur when the density of the inflow (e.g., turbid storm runoff) is higher than that of the water in the reservoir (Zavala, 2020). Large hyperpycnal flows would introduce oxic water into the bottom of the reservoir and impact carbon cycling. Dam reservoirs have unusual hydraulics compared to natural lakes (as the outflow exit is at the middle or bottom of the dam), and the role of outflow might affect thermal stratification and hypoxia but has received little attention so far. It is likely that microbial decomposition (aerobic and anaerobic) of autochthonous and allochthonous OM is the main contributor to oxygen depletion and source of GHGs within and from reservoirs (Rosa et al., 2004). Reservoir hypoxia is of increasing concern as it commonly harms aquaculture and other uses. Nutrient (mainly phosphate) in anoxic sediments may be released to overlying water and enhance eutrophication (Withers & Jarvie, 2008). The outflow discharge to downstream usually results in a lower DO below the environmental quality standard of surface water with unpredictable ecological consequences. However, the key physical and biological processes controlling seasonal oxygen dynamics and associated carbon cycling and export in reservoirs remain understudied. Therefore, a better understanding of the formation of hypoxia and the associated effect on CO_2 emission by reservoir systems is important to develop a better scientific basis for ecological protection and restoration of water resource in the basin.

China is one of the largest hydropower producers in the world (Ministry of Water Resources, 2013). Besides providing multiple benefits (flood control, electricity, irrigation, water supply, nutrient removal, carbon burial, etc.), the extensive hydropower development likely presents a long-term ecological and environmental risk due to eutrophication, hypoxia, and GHGs emission (Kumar et al., 2019b). Hundreds of dams have been built on the Min River (southeast China), among which Shuikou reservoir is the largest and is located furthest downstream, and hypoxia is of concern to fisheries and government. Given the fundamental differences between lake and reservoir systems (e.g., catchment, waterbody characteristics, and hydraulic features) (Hayes et al., 2017), the main question we seek to address is how oxygen consumption interacts with carbon cycling in a seasonal hypoxic reservoir. Here, we conducted a multidisciplinary study based on high-frequency observation of water quality in surface and bottom water, monthly profiling, and seasonal manual sampling and in situ incubations. The specific objectives of this study were to: (1) characterize the seasonal variation and vertical profile of dissolved oxygen (DO), CO_2, and other features within the reservoir; (2) examine the internal and external factors controlling oxygen consumption in the water column; and (3) reveal the seasonal imbalance between oxygen consumption and CO_2 emission.

2. Materials and Methods

2.1. Description of Study Site

The Min River is a subtropical river located in southeastern China (Figure 1). The basin has an area of 60,992 km² and is in a typical monsoon climate with strongly changing seasonal air temperature and precipitation. The mean annual air temperature is 16 °C–20 °C and about 70%–80% of the annual precipitation (1,700 mm) occurs in the wet season between April and September. The total river discharge in 2017 was about 48.2 billion m³. The geology of the basin is dominated by granite (silicate rock) with a stream pH of approximately 6.0–6.5 in the middle and lower reaches (Zhu et al., 2018). Shuikou reservoir is located in the lower Min River and has a total length of about 100 km, a dam height of about 101 m, and a water depth of about 60 m in the front of the dam with the outflow discharge at a depth of ~40 m to the bottom. The water capacity is 2.6 billion m³, the mean residence time is about 20 days, and the catchment to surface area ratio (CA:SA) is very large (524:1). According to Trophic State Index suggested by Carlson (1977), the

surface reservoir is classified as a mildly eutrophic system, but it suffers from a severe hypoxia problem in deeper water.

2.2. Sampling Campaign

The research targeted the lacustrine zone of the reservoir. Seven sites (S1–S7) in the lower Shuikou reservoir were selected for detailed study (Figure 1), and site S4 was chosen as the key site as it is located 8 km from the dam and is a typical location representing lacustrine features with less influence from dam operation. Four cruises were carried out in the reservoir, one in each season (April, August, November 2017, and January 2018). One additional sampling was performed in October 2018. Temperature (± 0.01 °C), DO (± 0.1 mg L^{-1}), and pH (± 0.01) profiles were made monthly at key site S4 and seasonally at all sites from June 2017 to January 2018 with a Multiparameter Water Quality Sonde (EXO2 Sonde, YSI). For depth profiling, the EXO2 Sonde was lowered slowly from the surface (0.5 m) to the bottom of the water (~ 1 m above sediments). Long-term monitoring of water quality was conducted in the surface and bottom water. Turbidity, water temperature, Chl-a, DO, and pH of surface water at site S4 were measured every 4 h (and the daily mean values were used in this study) by the national automatic water quality monitoring station under EPA China: water is pumped from the surface (0.5 m) of the reservoir into tanks wherein the sensors are deployed and maintained weekly. Water temperature, DO and pH in the bottom water were continuously monitored (from July 2018 to January 2018) in situ using another YSI Sonde which was bottom moored and surface tethered. To understand the emission of outflow CO_2, river sampling was performed at four sites (D1–D4) downstream of the dam during the peak period of CO_2 efflux in early November 2018 (before re-oxygenation in mid-November).

Discrete water samples were collected using a 5-L Niskin sampler at 0.5 m and below at depth intervals of 2–10 m (site S4 and S7). A total of 100-ml water was filtered in the field by a GF/F membrane and refrigerated at 4 °C until nutrient analysis was conducted within 2 days. Surface water from the reservoir (S1, S4, S7) and downstream river (D1–D4, only for fall 2018) and water column of sites S4 and S7 were collected for determination of pH, dissolved inorganic carbon (DIC) and total alkalinity (T_{alk}). DIC and T_{alk} were stored in a 40 mL brown glass vial and 125 mL high-density polyvinyl chloride bottle, respectively. After being poisoned upon collection with 1‰ saturated $HgCl_2$, the DIC and T_{alk} samples were analyzed within 1 week.

Surface (0–1 cm) sediments were collected with a Petite Ponar grab sampler at sites S4 and S7 in Shuikou reservoir during the spring dry season (April 2017) and summer wet season (August 2017). In the summer cruise (August 2017), we also collected sinking particles at site S4 using two cylindrical sediment traps (plexiglass tube with closed bottom, diameter 10 cm, height 60 cm) deployed at depths of 10 and 50 m during a period of 12 h. The traps were bottom moored and surface tethered (Gust & Kozerski, 2000). Traps were prefilled with high-density salt brine (40‰ NaCl) to prevent outflow and depress biological activity. Salt is not a treatment as strong as some other poisons (e.g., chloroform, formalin) for inhibiting bacterial activity (Lee et al., 1992), but for the short collection time used in this study, loss of particles due to biological activity should be reasonably small (Goto et al., 2016). After collection, samples were immediately filtered onto pre-combusted 25 mm-diameter GF/F filters. The sediment samples and filtered sinking particles were stored at 4 °C before physicochemical analysis.

2.3. Physicochemical Analysis

Filtered water was used to measure dissolved nutrient forms. Nitrate (NO_3-N), nitrite (NO_2-N), ammonium (NH_4-N), and dissolved reactive phosphorus (DRP) concentrations were measured with an AA3 Auto-Analyzer (SEAL, Germany), with detection limits of 0.1, 0.04, 0.5, and 0.02 μmol L^{-1}, respectively. Total dissolved phosphorus and nitrogen (TDP and TDN) were determined as NO_3-N and DRP following oxidization with 4% alkaline potassium persulfate. Dissolved organic P (DOP) was estimated by subtracting DRP from TDP, and dissolved organic N (DON) was obtained by subtracting DIN from TDN. The precision was estimated by repeated determinations of 10% of the samples and the relative error was 3%–5%. A standard reference material provided by China State EPA was used to check instrument performance.

Total suspended matter (TSM) was quantified by gravimetry. The oven-dried filter membranes were analyzed for total particulate phosphorus (TPP) after being combusted in a muffle furnace (550 °C for 1.5 h) and

extracted with 10 mL HCl (1M). Another set of water samples were filtered through 25 mm GF/F membranes for measurement of Chl-*a*. The filters were extracted with 90% acetone, and Chl-*a* was measured with a Turner fluorescence spectrophotometer.

Sediment samples were freeze-dried and ground, and a subsample was transferred to a 50-mL centrifuge tube. Excess organic-free 1-M HCl was added directly to samples to remove inorganic carbonate (Froelich, 1980), then combusted to determine the content of total organic carbon (TOC) and total nitrogen (TN) using an element analyzer (PE2400 SERIESIICHNS/O).

2.4. Oxygen and Carbonate System Analysis and CO_2 Efflux Estimation

DO concentration in discrete samples were determined using the Winkler procedure (Langdon, 2010) with a relative uncertainty of <0.5%, as determined from replicate analysis of a known NaS_2O_3 titration reagent concentration. O_2 depletion (ΔO_2) was calculated as the difference between the concentration in equilibrium with the atmosphere and the measured DO concentration (Benson & Krause, 1984).

DIC concentrations were determined by CO_2/H_2O analyzer (LI 7000) (Cai et al., 2004). T_{alk} was determined by an automatic titrator using a classical Gran titration method (Cai et al., 2004). The precision of DIC and T_{alk} was ±2 µmol kg^{-1}. pH was measured by a pH meter (Rex PHSJ-4F) with a precision of ±0.002. CO_2 concentrations in water samples were calculated based on measured pH and DIC through the CO2SYS program (Lewis & Wallace, 1998). Excess CO_2 (ΔCO_2) was calculated as shown in Equation 1; see the detailed description of the calculation in Zhai et al. (2005).

$$\Delta CO_2 = CO_{2(water)} - K_H CO_2 \times pCO_2 \left(\text{in air} \right) \tag{1}$$

where $CO_{2\,(water)}$ is the measured concentration of dissolved $CO_{2\,(water)}$ (µmol L^{-1}) in water; $K_H CO_2$ is the solubility coefficient of CO_2 (Weiss, 1974); pCO_2 (in air) was calculated by the atmospheric CO_2 concentration (390 ppm).

The CO_2 efflux (F) across the water-air interface was calculated using Equations 2–5. This study used indirect methods for CO_2 flux estimation, and there are various factors in the estimation methods with the potential to cause errors; see the uncertainty analyses in Section 3.8.

$$F = k \times \Delta CO_2 \tag{2}$$

$$k = k_{600} \times \left(Sc \, / \, 600 \right)^{-1/2} \tag{3}$$

$$k_{600} = 2.07 + 0.215 U_{10}^{1.7} \tag{4}$$

$$Sc = 1911.1 - 118.11t + 3.4527t^2 - 0.04132t^3 \tag{5}$$

where k is the gas transfer value at the observed temperature; k_{600} is the gas exchange coefficient at 20 °C (Cole & Caraco, 1998); U_{10} was the seasonal mean wind speed recorded at the nearest meteorological station; the Schmidt number (Sc) for CO_2 in freshwater varies with temperature (Wanninkhof, 1992); t is the observed water temperature.

We assumed that excess CO_2 produced in the reservoir would ultimately escape to the atmosphere through the water-air interface. The excess CO_2 near surface water of the reservoir can be emitted directly by exchange with the atmosphere as addressed by Equation 2, then the amount of outgassing CO_2 can be counted by the reservoir area (Equation 6). Excess CO_2 at deeper water is likely emitted through the outflow. Equation 2 is not applicable for estimation of outgassing CO_2 in the downstream water since CO_2 changed quickly with distance and the surface area of the downstream river is incalculable. Instead, the amount of outgassing CO_2 from outflow was quantified by Equation 7.

$$\text{Outgassing } C \left(\text{reservoir} \right) = \Sigma F_i \times S \tag{6}$$

$$\text{Outgassing } C\left(\text{outflow}\right) = CO_2\left(\text{water column}\right) \times Q \qquad (7)$$

where F_i is CO_2 efflux for each season; S is the area of Shuikou reservoir (94 km^2); ΔCO_2 (water column) is the average for the whole column; Q is the recorded discharge of dam outflow.

### 2.5. In Situ Incubation Experiments

2.5.1. Net Community Oxygen Production and Consumption Rates

Using a Niskin sampler, water was collected at four different depths (site S4) in the surface layer (at depths of 0–4 m corresponding to 100%, 30%, 5%, and 1% surface light intensity), in the middle (30 m), and in the bottom layer (60 m). The surface layer covered the epilimnion and metalimnion, and the middle and bottom layers corresponded to the hypolimnion. At each depth, nine pre-cleaned DO bottles (60 mL) were filled, and three bottles immediately received fixative to determine the initial concentration of dissolved oxygen. Three transparent bottles and three dark bottles wrapped with aluminum foil were redeployed in situ at the depth of collection and attached to a cable running from an anchor at the reservoir floor to a buoy at the surface. The incubation lasted from sunrise to sunset (Delille et al., 2005). The respiration rates (community respiration, CR) were calculated as the dark bottle change in oxygen and net community production (NCP) as the oxygen change in the transparent bottle. Gross primary production (GPP) was calculated from NCP plus CR (i.e., we assumed that respiration in the light and dark was similar).

2.5.2. Nitrification Oxygen Demand and Microbial Respiration Oxygen Demand in the Water Column

Nitrification rates were measured using an inhibitor technique, which has been successfully applied in both freshwater and estuarine water (Dai et al., 2008; Feray et al., 1999). Water samples were collected using a 5L Niskin sampler near the surface (0.5 m), middle (30 m), and bottom (60 m) of the water column. At each depth, nine brown bottles (250 mL) were filled: three control samples without adding any inhibitors; three bottles which received adequate ATU (final concentration of 100 mg L^{-1}) to inhibit the oxidation of ammonia (NH_4^+) to nitrite (NO_2^-); and three bottles which received $NaClO_3$ (final concentration of 10 mg L^{-1}) to inhibit the oxidation of NO_2^- to nitrate (NO_3^-). All bottles were redeployed at the depth of collection for in situ incubation for 24 h.

The oxygen demand by the two nitrification processes, ammonia oxidation (AO) and nitrite oxidation (NO), were estimated from the evolution of NO_2-N concentrations in bottles during the incubation. The nitrification-induced oxygen demand (NOD = AO + NO) was calculated using a stoichiometric approach based on the simplified nitrification reactions a and b (He et al., 2014).

$$NH_4^+ + 1.5O_2 \rightarrow NO_2^- + 2H^+ + H_2O \qquad (a)$$

$$NO_2^- + 0.5O_2 \rightarrow NO_3^- \qquad (b)$$
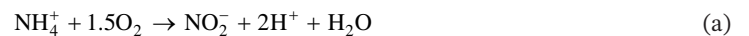
Microbial respiration oxygen demand (MOD) was calculated from total oxygen demand (TOD = CR) minus NOD.

3. Results

3.1. Meteorological Data and Water Quality Parameter of Surface Water and Bottom Water

The Shuikou Reservoir experienced four major rainstorm events in 2017 (i.e., events with 24-h precipitation greater than 50 mm), on April 21, June 16, July 31, and September 12 (marked as storm 1, 2, 3, and 4 in Figure 2a). Depending on the antecedent precipitation conditions and dam regulation, some rainstorms may cause high loadings of particulate matter through storm runoff into the river, which increases the turbidity of the reservoir (Figure 2b).
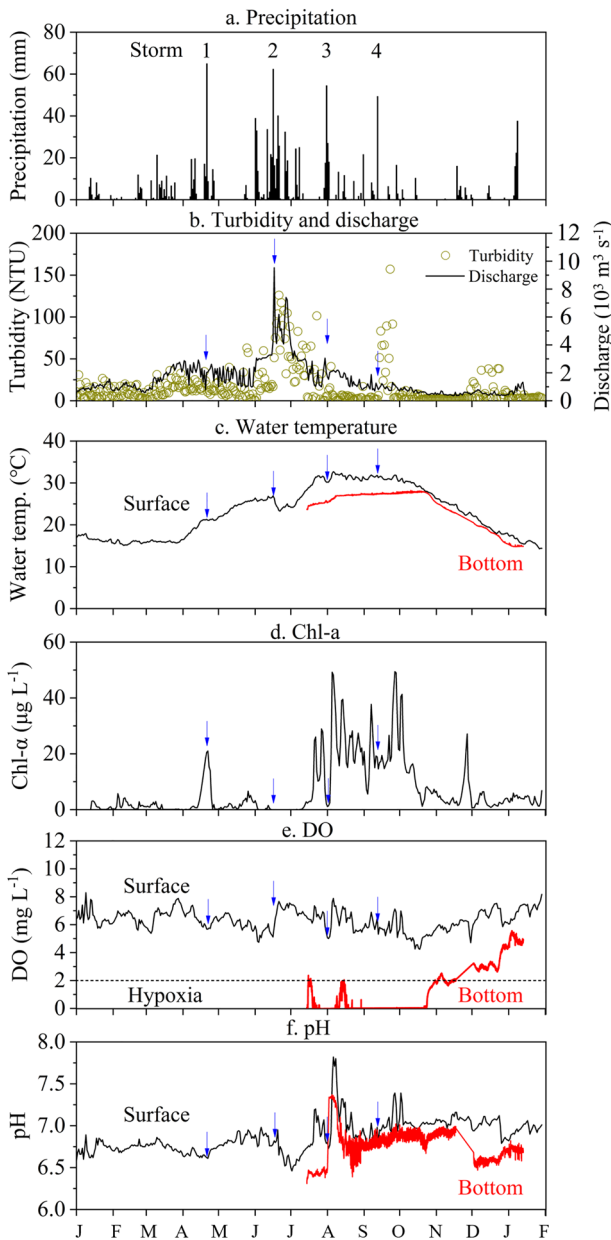
Figure 2. Meteorological data and water quality parameter (a-f) of surface water (from January 2017 to January 2018) and bottom water (from July 2017 to January 2018) at site S4 in the Shuikou reservoir. Small arrows indicate timing of major rain storm events.

In late summer (July–August) the bottom water temperature was 4 °C–6 °C cooler than the surface water (Figure 2c). The maximum thermal difference occurred at the end of July, indicating that the thermal stratification was severest at this time. Thereafter, the thermal difference decreased gradually to less than 0.5 °C in late October. The Shuikou reservoir also experienced algae blooms (chlorophyll-a > 10 μg L^{-1}) from mid-July to mid-October (Figure 2d), which caused peaks of DO and pH values in the surface water (Figures 2e and 2f). The change of turbidity caused by high abundance of phytoplankton during algal bloom was much less notable than the flood impact. The DO concentration ranged from 4.24 to 8.29 mg L^{-1} in surface water (mostly below saturation levels) and 0.05–5.56 mg L^{-1} in bottom water during the measurement periods (Figure 2e). It appeared that the heavy rainstorms caused short pulses of oxygen in the bottom water during the July-August period, but otherwise the bottom water remained hypoxic before re-oxygenating in mid-November.

3.2. Seasonal Stratification of Water Temperature, Dissolved Oxygen, and pH

Monthly variation of temperature, pH, and DO at site S4 in Shuikou reservoir monitored by the YSI profiler during 2017–2018 are shown in Figure 3. Water temperature ranged from 14 °C to 32 °C with surface waters in September being the warmest, and bottom waters in January being the coldest. Figure 3 illustrates the progressive development of thermal stratification starting in mid-July (summer). Two thermoclines (defined as the depth intervals with a gradient larger than 0.2 °C m^{-1}) appeared in the water column: the surface thermocline at ~2 m, and the deeper thermocline at ~40 m (Figure 3). The surface thermocline gradually deepened and the deeper one shallowed before they merged together in mid-November (fall). The water was completely mixed and the thermocline disappeared in January.

The DO concentration ranged from 0 to 9 mg L^{-1} and its pattern was consistent with the observed water stratification (Figure S3). Bottom water was hypoxic (DO < 2 mg L^{-1}) to anoxic (DO < 0.2 mg L^{-1}) for as much as four months (July to November 2017). Oxyclines, defined as the depth intervals with a gradient larger than 0.2 mg L^{-1} m^{-1}, mirrored the thermoclines during the summer and fall and disappeared in early December (Figure 3). DO in the surface water was supersaturated from early July to August (Figure S3d), accompanied by the phytoplankton blooms (Figure 2d). The pH ranged from 6.2 to 7.6 in the stratification period, with lower bottom-water pH values during the hypoxic period (Figure S3b).

The longitudinal profile of DO along the river-reservoir gradient (Figure 4) also showed thermal stratification and widespread distribution of hypoxia in summer in both years (2017 and 2018). Higher DO could be found in the bottom water receiving tributary inflows between S6 and S5.

3.3. Vertical Distribution of DIC, T_{alk}, ΔCO$_2$, and Dissolved Nutrients in the Water Column

The vertical profiles show the variation of the carbonate system in the Shuikou reservoir at site S4 and S7 during the seasons (Figure 5). The concentration of CO$_2$ in the water column was undersaturated in the surface (0.5 m) water during summer. ΔCO$_2$ varied from −9.4 to 180 μmol L^{-1} and −8.4 to 117.4 μmol L^{-1} in the water column at site S4 and S7 respectively, and ΔCO$_2$ in fall and winter were greater than that in spring
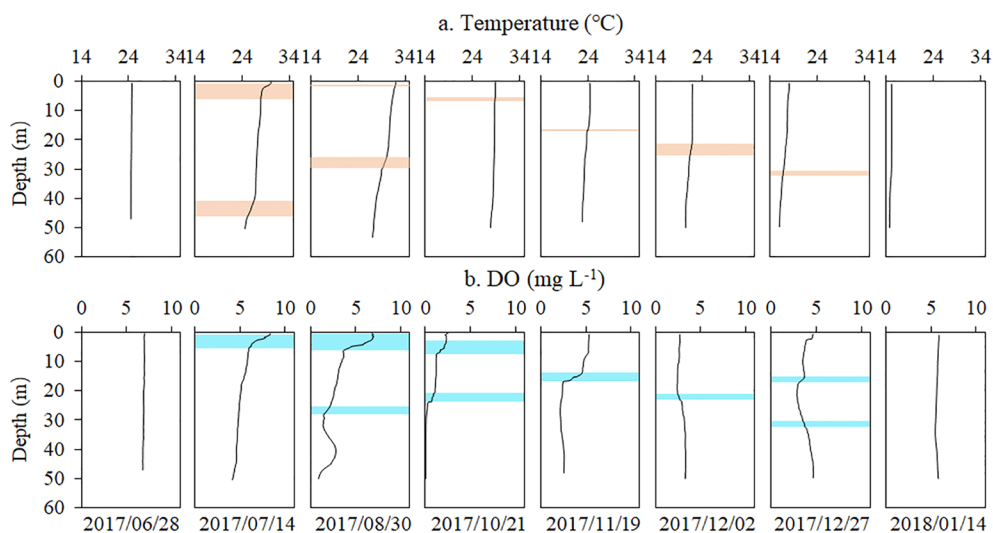
Figure 3. Vertical profile of temperature (a) and DO (b) at site S4 in the Shuikou reservoir (2017–2018). Thermocline and oxycline thickness indicated by shaded rectangles. The thermocline and oxycline was defined as the vertical gradient of water temperature and DO be greater than 0.2 °C m^{-1} and 0.2 mg L^{-1} m^{-1}.

and summer (Figure 5a). The concentration of DIC in the water column varied greatly between the four seasons (200–750 μmol L^{-1}). In spring and winter, DIC was evenly distributed due to water mixing, although the concentration measured in the bottom water was somewhat higher than the surface water (Figures 5b and 5e). In summer the T_{alk} values measured in the upper (<5 m) water (300–450 μmol L^{-1}) were lower than the values determined in the deep water (379–556 μmol L^{-1} at site S4 and 378–542 μmol L^{-1} at site S7). T_{alk} differed little from surface to bottom in spring and winter (Figures 5c and 5f).

Vertical profiles of dissolved nutrients, DO and Chl-*a* concentrations are shown in Figure 6. During the summer with stratified conditions, high concentrations of DO, Chl-*a*, TPP, DOP, and DON and low concentrations of NH$_4$-N and SRP were observed in the euphotic zone (0–5 m). NH$_4$-N declined downward from a peak at 5 m but increased again in bottom water. In contrast, NO$_3$-N changed little above 30 m but decreased quickly to the bottom. By contrast in winter, most parameters were evenly distributed in the water column except for NH$_4$-N and TSM, which increased with water depth.

3.4. Oxygen Metabolism in the Water Column

3.4.1. GPP and CR in the Euphotic Zone

GPP ranged from 15.6 to 125.3 μmol O$_2$ L^{-1} d^{-1} in summer and 6.9–15.7 μmol O$_2$ L^{-1} d^{-1} in winter (Table 1). GPP in the euphotic layer decreased sharply with depth and followed the light percentage with a monod-type curve during both winter and summer. GPP in summer was about 8 times higher than in winter during the period when there was a large phytoplankton biomass (as determined by Chlorophyll-*a* content) and intense solar radiation. CR ranged from 49.4 to 68.1 μmol O$_2$ L^{-1} d^{-1} in summer and 9.2–31.0 μmol O$_2$ L^{-1} d^{-1} in winter, and CR decreased with depth whatever the season. In summer, the depth-integrated GPP in the euphotic zone was 262.7 μmol O$_2$ m^{-2} d^{-1} and the CR was 216.7 μmol O$_2$ m^{-2} d^{-1}, and in winter, the GPP was 49.0 μmol O$_2$ m^{-2} d^{-1} and CR was 68.7 μmol O$_2$ m^{-2} d^{-1}.

3.4.2. Nitrification Oxygen Consumption and Microbial-Respiration Oxygen Consumption

The in situ AO (ammonium oxidation oxygen demand) in summer was undetectable in the whole water column and ranged from 0.43 to 1.44 μmol O$_2$ L^{-1} d^{-1} in winter (Table 2). NO (nitrite oxidation oxygen demand) ranged from 0.01 to 0.37 μmol O$_2$ L^{-1} d^{-1} in summer and 0.10–0.56 μmol O$_2$ L^{-1} d^{-1} in winter. NO was much higher than AO in summer while AO was higher than NO in winter, with the exception of bottom water. The MOD (microbial respiration oxygen demand) ranged from 10.23 to 68.05 μmol O$_2$ L^{-1} d^{-1} in summer and from 2.04 to 30.41 μmol O$_2$ L^{-1} d^{-1} in winter (Table 2). MOD was higher in summer than
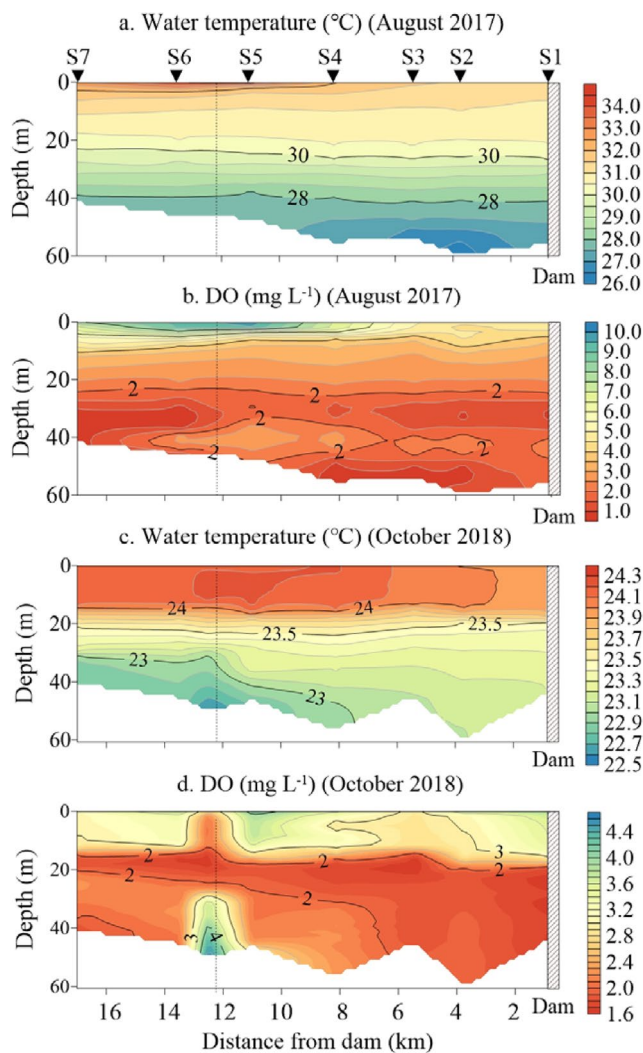
Figure 4. Longitudinal cross-section distributions of temperature and DO in the Shuikou reservoir in August, 2017 (a-b) and October, 2018 (c-d). Dashed lines indicate the location of tributary.

in winter, contributing more than 96.5% to total oxygen demand (i.e., CR). In winter, MOD accounted for 98.1% of CR in surface water but only 68.0% in bottom water.

3.5. Sediment and Sinking Particle Carbon and Nitrogen

The content of TOC and TN and the C:N mass ratio in surface sediments varied with season and site (Table 3). TOC and TN in top sediments (0–0.5 cm) were higher in summer (wet season) than in spring (dry season) and changed little in the sediments below (0.5–1.0 cm). The C:N ratios of top sediments were lower in summer (7.1–9.2) than in spring (12.3–13.4). Site S4 (closer to dam) had a higher TOC and TN than site S7, and also had a lower C:N ratio than site S7, particularly in summer. Sinking particles collected at site S4 (10 m depth) had a C:N ratio of 5.77 (Table 4), while particles collected at 50 m depth had a C:N ratio of 7.12, similar to that of surface sediments (Table 3). Particle fluxes increased with water depth (Table 4).

3.6. Excess CO_2 versus O_2 Depletion Below the Euphotic Zone

The seasonal $\Delta CO_2/\Delta O_2$ ratios at site S4 and S7 below the euphotic zone fell into three different groups (Figure 7). The average $\Delta CO_2/\Delta O_2$ ratios were 0.88 ± 0.03 and 0.97 ± 0.14 during spring and fall at site S4, fairly similar to site S7 (0.84 ± 0.14 and 0.95 ± 0.05 respectively) and close to the expected range of 0.62–0.90 (Elser et al., 2000; S. Wang et al., 2015). During summer the observed $\Delta CO_2/\Delta O_2$ ratio was very low and below the expected range at sites S4 and S7 (0.43 ± 0.08 and 0.50 ± 0.05 respectively). In winter, the observed $\Delta CO_2/\Delta O_2$ ratio were higher than the upper limit of the expected range at sites S4 and S7 (1.09 ± 0.07 and 0.99 ± 0.07 respectively).

3.7. Efflux of CO_2 in Shuikou Reservoir and Downstream River

The averaged water-air CO_2 flux from the reservoir (sites S1, S4, and S7) was 36.2 mmol $m^{-2}d^{-1}$ in spring, -6.7 mmol $m^{-2}d^{-1}$ in summer, 89.7 mmol $m^{-2}d^{-1}$ in fall, and 58.8 mmol $m^{-2}d^{-1}$ in winter (Figure 8a). The water-air CO_2 flux in fall decreased quickly from 87.8 to 41.9 mmol $m^{-2}d^{-1}$ with increasing distance downstream from the dam (Figure 8b). Assuming the excess CO_2 from dam outflow will finally be emitted to the atmosphere and reach equilibrium, the total outgassing of CO_2 in reservoir and downstream was estimated as 5.7×10^7 kg C yr^{-1} (Table 5), of which the reservoir accounted for 32% and outflow accounted for 68%. There were also seasonal differences in CO_2 emission: in summer, reservoir surface water appeared to be a CO_2 sink, but CO_2 remained oversaturated in deeper water and outflow was a relative weak source; in other seasons, outgassing of CO_2 from outflow was greater (strong source) than from the reservoir surface (Table 5).

3.8. Uncertainty Analyses of CO_2 Efflux Estimation

Using indirect methods for CO_2 estimation leads to inescapable errors. First, measured gas fluxes often differ significantly from gas transfer coefficients. For example, Heiskanen et al. (2014) show the effects of cooling and internal wave motions on gas transfer coefficients in a boreal lake. Schwefel et al. (2016) found that values calculated by Cole and Caraco (1998) were too low and had to be increased artificially by a calibration parameter. A larger error comes from the different k_{600} formulas in this study (Equation 4) compared with others (Equations 8–10) (Crusius & Wanninkhof, 2003; Guérin et al., 2007; Raymond & Cole, 2001). The
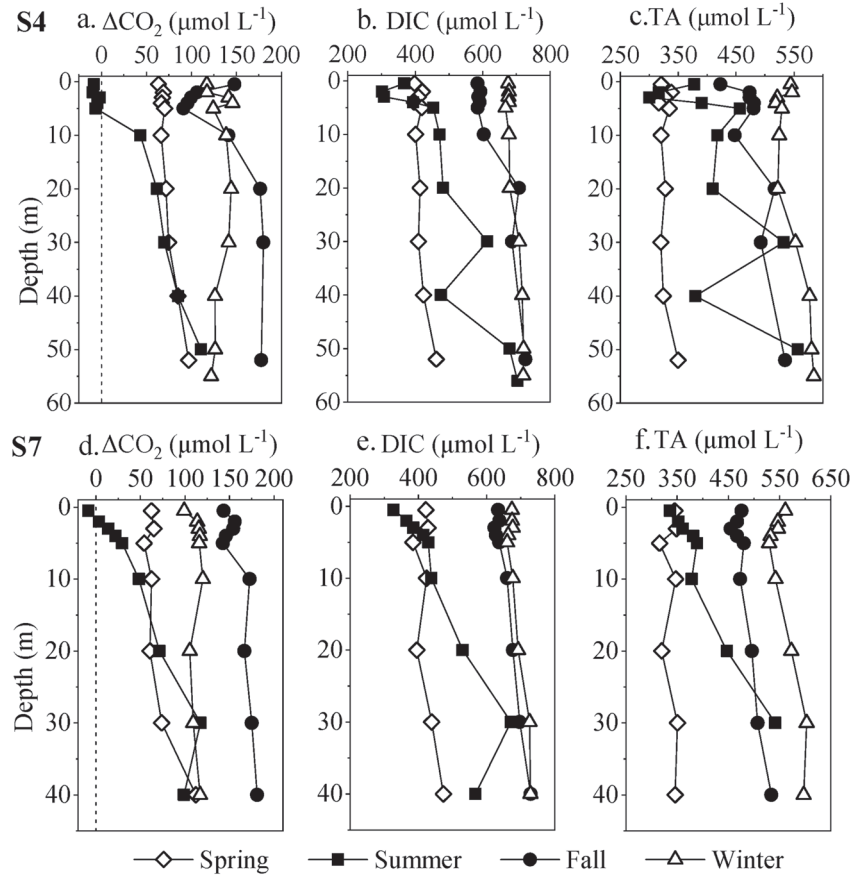
Figure 5. Vertical distribution of ΔCO_2, DIC, and TA in four seasons (April, August, November 2017, and January 2018) at site S4 (a–c) and S7 (d–f) in the Shuikou reservoir. DIC, dissolved inorganic carbon;.

averaged CO_2 efflux using these k_{600} was 31.1 ± 17.3 mmol m^{-2} d^{-1} in spring, −6.0 ± 3.2 mmol m^{-2} d^{-1} in summer, 76.4 ± 43.0 mmol m^{-2} d^{-1} in fall, and 50.5 ± 28.2 mmol m^{-2} d^{-1} in winter, with the lowest estimated flux using the Wanninkhof method (Figure S4). The relative deviation between the estimation using seasonally averaged wind speeds and the wind speed of the sampling day was 1.6% in spring, −2.7% in summer, −0.4% in fall, and 1.4% in winter. Wind speed (U_{10}) is also an important factor in estimating CO_2 efflux. The relative deviation between the estimation using seasonally averaged wind speeds and the wind speed of the sampling day was 3.2% in spring, −5.4% in summer, −0.8% in fall, and 2.8% in winter. Second, there were errors of less than 1.1% in CO_2 efflux resulting from the measurement precision of pH and DIC (Table S2). Third, the seasonal sampling might also produce potential errors compared with high-frequency measurements. Although a correlation between the discrete sampling of pH and CO_2 exists it varied between seasons (Figure S2). In the absence of a long-term in situ measurement of pH in surface water (measurement of pumped water), we evaluated the seasonal variation (one standard deviation) of pH measurement, and then estimated the seasonal variation of CO_2 efflux to be 35.5 ± 7.1 mmol m^{-2} d^{-1} in spring, −6.3 ± 1.5 mmol m^{-2} d^{-1} in summer, 90.9 ± 18.2 mmol m^{-2} d^{-1} in fall, and 60.9 ± 10.3 mmol m^{-2} d^{-1} in winter at site S4 (Table S3). Accordingly, the errors of estimated seasonal CO_2 efflux were 20%, 24%, 20%, and 17% respectively. All these error analyses suggest that our estimation of CO_2 efflux using Equation 4 were reliable and comparable.

$$k_{600} = 0.228\,U_{10}^{2.2} + 0.168 \tag{8}$$

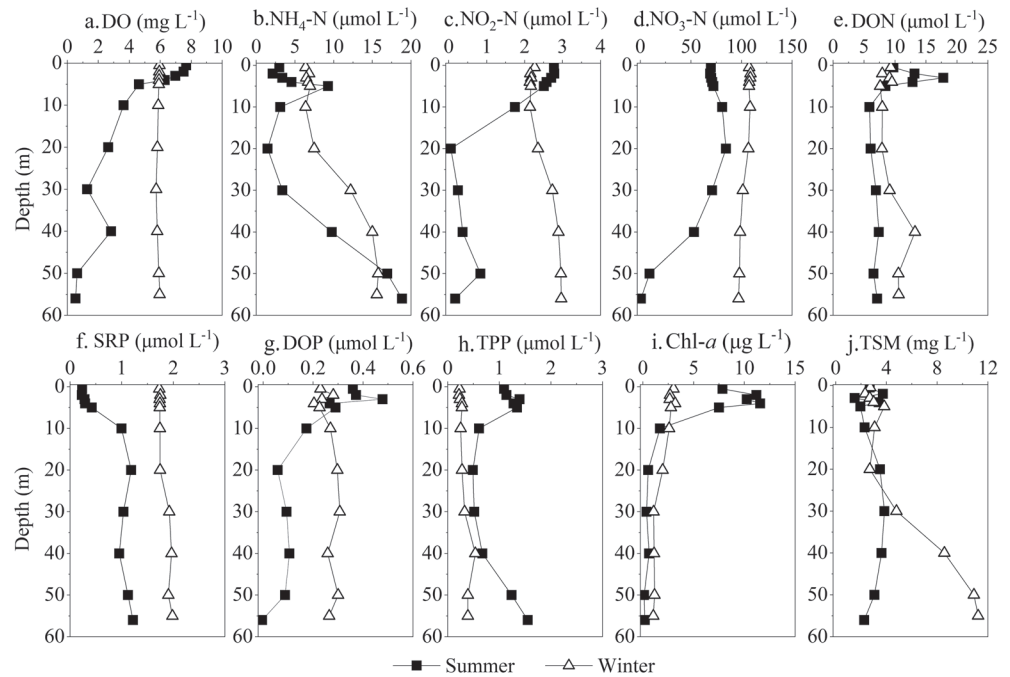$$k_{600} = 1.76 + 0.23\,U_{10}^{1.78} \tag{9}$$

Figure 6. Vertical distribution of DO (a), nutrients (b-h), Chl-a (i) and TSM (j) in summer and winter (August 2017 and January 2018) at site S4 in the Shuikou reservoir.

$$k_{600} = 2.06 \exp^{(0.37 \times U_{10})} \tag{10}$$

4. Discussion

4.1. External Controls on Seasonal Hypoxia and Oxygen Imbalance

In 2017, the hypoxia in the studied reservoir was sustained for four months from mid-July (summer) to mid-November (late fall), and the hypoxia zone expanded from the bottom to near surface water (5 m) by mid-October (Figure 4). There were two thermoclines in the water column of the reservoir (Figure 3). The upper thermocline at ~2 m was a result of lower density water warmed by solar radiation compared to subsurface water. The deeper thermocline initially formed in July due to the strong temperature gradient between the middle and bottom hypolimnion. Thereafter it rose to a depth of about 40 m, likely due to the increased advective river flow toward the outflow from the reservoir, which is situated at a depth of 40 m in the middle of the dam. Decreasing temperatures from fall into winter increased the depth of vertical

Table 1
GPP and CR in Euphotic Layer of the Shuikou Reservoir (Site S4)

Depth (layer)	GPP ($\mu mol\ O_2\ L^{-1}\ d^{-1}$)		CR ($\mu mol\ O_2\ L^{-1}\ d^{-1}$)		GPP/CR ratio	
	Summer	Winter	Summer	Winter	Summer	Winter
100% light intensity	125.3 ± 1.9	15.7 ± 0.1	68.1 ± 0.1	31.0 ± 0.6	1.8 ± 0.03	0.5 ± 0.05
30% light intensity	114.5 ± 3.8	12.7 ± 1.4	53.7 ± 4.2	17.9 ± 2.0	2.1 ± 0.12	0.7 ± 0.03
5% light intensity	67.2 ± 1.5	9.6 ± 0.2	51.2 ± 8.9	10.3 ± 2.9	1.3 ± 0.08	0.9 ± 0.07
1% light intensity	15.6 ± 0.2	6.9 ± 0.5	49.4 ± 1.1	9.2 ± 2.3	0.3 ± 0.02	0.8 ± 0.07

Note: The incubation time was ~12 h in summer and ~10 h in winter, from sunrise to sunset.
Abbreviations: CR, community respiration; GPP, gross primary production.

Table 2
Summary of In Situ Incubation Derived Oxygen Demand in the Shuikou Reservoir (Site S4)

| Cruises | Water layer | Initial DO (μmol O_2 L^{-1}) | TOD (μmol O_2 L^{-1} d^{-1}) | NOD (μmol O_2 L^{-1} d^{-1}) | | MOD (μmol O_2 L^{-1} d^{-1}) | MOD/ TOD (%) |
				AO	NO		
Summer	Surface	276.6	68.1	<0.1	<0.1	68.05	99.9
	Middle	41.5	18.1	<0.1	<0.1	18.09	99.9
	Bottom	16.7	10.6	<0.1	0.37	10.23	96.5
Winter	Surface	192.7	31.0	0.43	0.16	30.41	98.1
	Middle	180.4	7.5	1.44	0.10	5.96	79.5
	Bottom	176.0	3.0	0.40	0.56	2.04	68.0

Notes. TOD represents the total oxygen demand, refers to CR in Table 1; NOD represents the nitrification oxygen demand; AO represents the ammonium oxidation oxygen demand; NO represents the nitrite oxidation oxygen demand; MOD represents the microbial respiration oxygen demand, which is calculated as TOD minus NOD.

mixing and decreased the vertical temperature gradient, and the surface thermocline gradually deepened as a consequence. In winter, the two thermoclines disappeared and the water was completely vertically mixed.

The two thermoclines prevented the oxygen supply from surface water reaching the hypolimnion despite the surface water being oxic and even over-saturated due to strong photosynthesis during phytoplankton blooms in summer and fall (Figures 2–4). In some cases, additional oxygen may be supplied by hyperpycnal flow near the bottom (Figure 2e), leading to another oxycline forming in deeper water, even though sometimes the temperature gradient was relatively weak (e.g., in October 2017) (Figure 3). As shown in the longitudinal profile of DO along the river-reservoir gradient (Figure 4), a tributary between S6 and S5 seems to have introduced high-density oxic water near the bottom of the reservoir; this water was from a small cool stream shaded by riparian vegetation. In addition, storm-induced flood water (which contained a high density of particles) might have supplied external oxygen to the deep water. As shown in Figure 2e, two pulses of increased bottom water DO were observed in the hypoxic layer following rainstorms. Such hyperpycnal flow from cool tributary and/or flood water seems to have temporarily reduced the hypoxic conditions in the deeper waters. Nevertheless, hypoxia did not disappear during the summer and fall periods, implying that there were insufficient partially oxygenated inputs of "new" oxic water to overcome the large oxygen deficit in the deeper water column.

The average draining ratio (CA:SA) is 3–4 times greater in reservoirs than lakes (Harrison et al., 2009), and greater CA:SA likely results in higher nutrient and sediment inputs to reservoirs (Hayes et al., 2017). Shikou reservoir is obviously a river-dominated system receiving externally supplied OM because its CA:SA is very high (524:1). Turbidity peaked in summer with particularly high river flow periods caused by rainstorms (Figure 2a). According to the regression of the measured TSM on sensor-based turbidity ([TSM] = 1.2549 × [turbidity] + 0.5344, R^2 = 0.96, Figure S1), the time series of TSM at site S4 could be

Table 3
Content of Total Organic Carbon, Total Nitrogen, and C:N Ratio in Surface Sediments in the Shuikou Reservoir

Site	Season (month)	Layer (cm)	TOC (g kg^{-1})	TN (g kg^{-1})	C:N mass ratio
S4	Spring/dry season (April)	0–0.5	18.50	1.50	12.33
		0.5–1	16.90	1.40	12.07
	Summer/wet season (August)	0–0.5	20.21	2.83	7.14
		0.5–1	16.60	1.71	9.73
S7	Spring/dry season (April)	0–0.5	16.60	1.30	12.77
		0.5–1	16.10	1.20	13.42
	Summer/wet season (August)	0–0.5	19.14	2.09	9.18
		0.5–1	15.21	1.32	11.50

Table 4
Sinking Rate of POC, PON, and C:N Ratio in Sinking Particles in the Shuikou Reservoir (Site S4)

Site	Season (month)	Water layer (m)	Sinking POC (mg $m^{-2} h^{-1}$)	Sinking PON (mg $m^{-2} h^{-1}$)	C:N mass ratio
S4	Summer (August)	0–10	3.67	0.64	5.77
		0–50	9.86	1.39	7.12

estimated. The TSM load (product of daily mean TSM concentration and flow rate) in summer (June 1–August 31) accounted for 43% of annual load. Heavy rainfall events could bring large amounts of nutrients and eroded particulate matter into the reservoir from the mountainous catchment (Huang et al., 2014). Although we did not measure the content of OM of the TSM, it is evident that a large amount of OM was transported into the reservoir via storm runoff in summer. This external OM can be trapped behind the dam and cause microbial consumption of oxygen in subsequent seasons (see more discussion below).

4.2. Internal Controls on Oxygen Consumption

Oxygen consumption in the water column is mainly due to microbial respiration of OM (Mackenthun & Stefan, 1998), nitrification, and oxidation of other reductive substances (Matthews & Effler, 2006; Zaw & Chiswell, 1999). The results from in situ incubation showed that microbial respiration (MOD) was the major contributor to oxygen consumption (67.4%–99.9%) (Table 2). In summer, the nitrification contribution (NOD) was minor largely due to the low NH_4-N concentrations, but was more apparent in winter when the bottom water became oxic (Figure 6a) after a period of NH_4-N accumulation (Figure 6b). In contrast, microbial respiration (MOD) may be reduced in winter when the temperature is falling and the OM supply decreases (i.e., lower GPP and runoff input). Although benthic nitrification is another process consuming oxygen (Deemer et al., 2011), we speculated that nitrification could be limited in anoxic sediments and did not measure it. In summer, very low DO was observed in bottom water except when storms induced hyperpycnal flow (Figure 2e). A significant increase in NH_4-N and decline of NO_2-N and NO_3-N with water depth was observed in summer (Figure 6), implying that benthic nitrification was restricted but that denitrification could be active. In winter, vertical mixing allows oxygen to be supplied to deeper water and supports benthic nitrification. A study in a mesotrophic lake showed that nitrification in the sediment and in the water column made approximately equal contributions to the total areal oxygen deficit, and the benthic nitrification accounted for less than 10% of the total oxygen depletion (Hall & Jeffries, 1984). We concluded that the contribution of nitrification to oxygen consumption is relatively unimportant in Shuikou reservoir and other similar hypoxia systems.

The GPP/CR ratio can be used to evaluate the metabolic status of a water body: if the GPP/CR ratio is less than 1, external (allochthonous) OM supports the respiration of the aquatic ecosystem; if the GPP/CR ratio is higher than 1, in situ primary production provides more OM than is consumed locally (Hanson
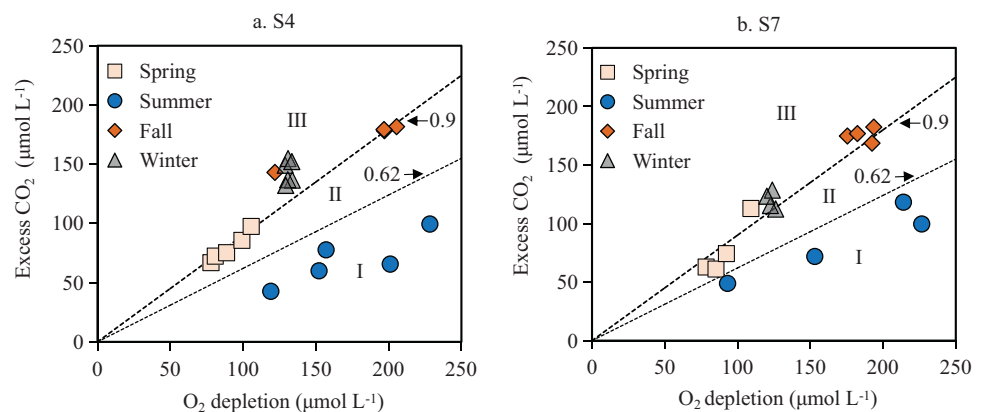

Figure 7. Excess CO_2 versus O_2 depletion in four seasons (April, August, November 2017, and January 2018) below the euphotic zone at site S4 (a) and S7 (b) in the Shuikou reservoir. The O_2 depletion caused by nitrification in the middle and bottom layers in January 2018 have been corrected by the ratio of MOD to TOD (refer to Table 2). The numbers (0.62–0.9) indicate the expected range of mole ratios of excess CO_2 to O_2 depletion ($\Delta CO_2/\Delta O_2$) ratio in freshwater (Elser et al., 2000; S. Wang et al., 2015).
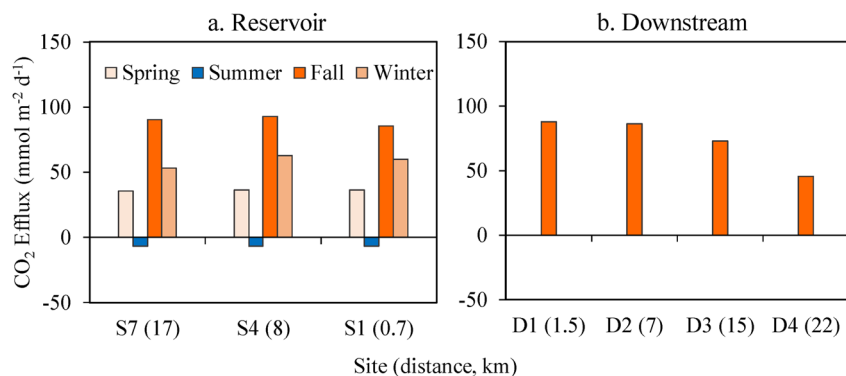
Figure 8. Water-air flux of CO_2 in (a) Shuikou reservoir in four seasons of 2017 and (b) downstream of the dam (sites D1-D4 refer to Figure 1) in fall of 2018. Direct measurement of CO_2 in downstream in other seasons was not available but the outgassing was estimated based on the excess CO_2 in the water column and outflow discharge (refer to Table 5).

et al., 2003). In the Shuikou reservoir, the GPP/CR ratio of surface water with light intensity >5% in summer was higher (1.3–2.1) than in winter (0.5–0.9) (Table 1). The depth-integrated GPP/CR ratio during summer (1.21) indicated net autrotrophy for the euphotic zone, while the depth-integrated ratio during winter (0.71) indicated a dominance of respiration over primary production due to consumption of external or earlier-produced OM. The upper part of the euphotic zone (0–5 m) in summer was depleted in NH_4-N and SRP and had higher DO and Chl-*a* in summer (Figures 2d and 2e), indicating high primary production. The autochthonous OM produced in the euphotic layer was likely transferred to the deeper water and river bed and resulted in net consumption of oxygen and a negative metabolic balance in deeper waters.

The C/N ratio of higher plants is usually 13–14 and may even exceed 30 (Müller & Mathesius, 1999), while the C/N ratio of autochthonous lacustrine OM in lakes and reservoirs is relatively low (typically less than 10) (Giresse et al., 1994). In this study, the measured C/N ratio of the topmost sediments was lower in the summer wet season (<10) than in spring dry season (>12) (Table 3). The OM that survived through the winter into spring likely contained a larger fraction of allochthonous material. Further, the C/N ratio of sinking particles collected by the sediment trap at 10 m was about 5.8 (Table 4), which is consistent with the very high GPP in the euphotic zone in summer (Table 1). Primary production during summer was estimated at about 80 g C m^{-2}. If all this OM was exported to below the thermocline and respired, then oxygen would reach <2 mg L^{-1}, and this is expected because locally produced material enhances microbial respiration. If the organic carbon export measured at 10 m during summer is assumed to be constant over the year at 3.67 mg m^{-2} h^{-1}, it could consume 0.5 mg O_2 L^{-1}, which is one order of magnitude lower than the oxygen decrease we observed. Therefore, it can be inferred that the allochthonous material consumed most of oxygen below the thermocline.

4.3. Imbalance Between Oxygen Consumption and Carbon Dioxide Emission

For a specific water body, excess CO_2 (ΔCO_2) and O_2 depletion (ΔO_2) generally follow a fixed stoichiometric relation, namely $\Delta CO_2 / \Delta O_2 = 0.77$ (106/138 is the Redfield ratio [Redfield et al., 1963]), due to degradation of OM. Considering that the phytoplankton species of freshwater systems are different from those in marine

Table 5
The Outgassing of CO_2 Within the Reservoir and Dam Outflow

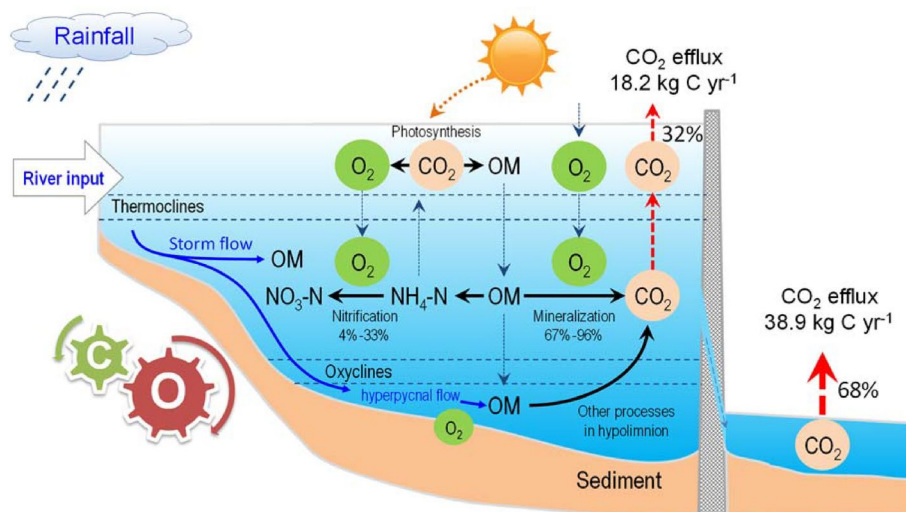| Item	Spring (10^6 kg C)	Summer (10^6 kg C)	Fall (10^6 kg C)	Winter (10^6 kg C)	Year (10^6 kg C)	Contribution (%)
Reservoir	3.7	−0.7	9.2	6.0	18.2	32
Outflow	12.1	6.4	10.0	10.4	38.9	68
Total	15.8	5.7	19.2	16.4	57.1	100

Figure 9. A conceptual schematic of interaction between oxygen consumption and carbon dioxide emission in a subtropical hypoxic reservoir.

systems (Elser et al., 2000), and that these generally have a higher proportion of lipids, one would expect about 36% more oxygen consumption for lacustrine than "typical" marine OM (Fraga et al., 1998). The common $\Delta O_2/\Delta CO_2$ ratio in freshwater has been reviewed to vary between 0.62 and 0.90 (Elser et al., 2000; S. Wang et al., 2015). During summer the observed $\Delta CO_2/\Delta O_2$ ratio (less than 0.62) was lower than in other seasons (Figure 7). This low $\Delta CO_2/\Delta O_2$ ratio could either be due to oxygen consumption not associated with CO_2 release or CO_2 consumption processes not involving oxygen. Chemoautotrophic processes using oxygen (and consuming CO_2) could potentially contribute to the observed low $\Delta CO_2/\Delta O_2$ ratio, but oxygen consumption due to nitrification was found to be very low (Table 2). Sedimentary release of reduced iron, manganese and sulfide and subsequent re-oxidation in deep waters could be an alternative explanation but we do not have data to constrain this. Benthic methane release and subsequent water-column oxidation would not contribute to low $\Delta CO_2/\Delta O_2$ ratios because for each mole of oxygen consumed one mole of CO_2 is produced. The low oxygen conditions in bottom water during summer (Figures 2–4) might have led to anaerobic degradation of OM. This does not involve consumption of oxygen but does increase alkalinity, with the consequence that ΔCO_2 declines due to chemical buffering (Middelburg, 2019). In winter, the observed $\Delta CO_2/\Delta O_2$ ratio was 1.31 ± 0.09, higher than the upper limit of the range expected for respiratory processes (0.92) (Figure 7). It should be noted ΔO_2 here represents the oxygen consumption by microbial respiration excluding nitrification (corrected by the ratio of MOD to TOD, Table 2). Enhanced vertical mixing by the cooling weather caused the breakdown of the stable thermal stratification in winter, so oxygen was replenished from the atmosphere to the water column. This oxygen supply to the low-oxygen, ammonium-rich bottom waters stimulated nitrification, and the enhanced biogeochemical processes of ammonium oxidation and nitrification, which were observed in the middle (NOD/TOD = 20.6%) and bottom (NOD/TOD = 32.6%) layers in winter (Table 2), produce more H^+. A negative correlation was observed between CO_2 and pH (Appendix Figure S2), suggesting that the extra CO_2 in winter might be due to bicarbonate titration by H^+ (i.e., proton buffering).

Current results suggest that the Shuikou reservoir serves as a net source of CO_2 to the atmosphere on an annual basis (Figure 8 and Table 5). Compared with other reservoirs around the world, Shuikou reservoir falls in the range of reported values (Table S1). During the summer period with high primary production, the reservoir temporarily acted as a sink of atmospheric CO_2 in the surface water, while the deeper waters remained oversaturated with respect to CO_2 (Figure 5a). The excess CO_2 will be transported downstream, exit the reservoir and eventually be released to the atmosphere from the outflow water (Figure 8b). The amount of outgassing CO_2 from the outflow (68% of total) is twice as large as from the reservoir itself (Table 5), and is a clear example of outgassing from imported excess CO_2. Other studies also suggest that rivers downstream from reservoirs are an important source for CO_2 emission to the atmosphere (Bevelhimer

et al., 2016; F. S. Wang et al., 2011). Overall, the Shuikou reservoir served as a net source of atmospheric CO_2, both directly and indirectly via export of CO_2-rich outflow waters. The emission of CO_2 downriver of dam reservoirs deserves further research to better understand the role of the reservoir in processing riverine carbon during its export from the watershed to coast.

5. Conclusions

Hypoxia was found to last for four months from summer to fall (July-November) in the Shuikou reservoir, and to expand from the bottom water to close to the surface. The water column included two thermoclines ($\sim$2 and $\sim$40 m), which prevented oxygen supply from surface water reaching the hypolimnion, and allowed external OM supplied by rainstorm runoff to consume most of the oxygen in the deeper water. In addition, the export of high primary production in summer contributed to additional OM supply to the deeper water in the reservoir. The degradation of autochthonous and allochthonous OM played a vital role in microbial oxygen consumption, while nitrification was shown to make a smaller contribution. We observed an imbalance between oxygen consumption and CO_2 emission in summer and winter, likely due to other biogeochemical processes (chemoautotrophy, anaerobic degradation of OM, proton buffering, and nitrification). The water-air fluxes confirm that the reservoir is a net source of CO_2 except for summer when primary production is high. In addition to the direct emission of CO_2 within the reservoir, the river downstream of the reservoir also acted as a major source of CO_2 as the dam outflow was oversaturated with CO_2. A conceptual schematic of interaction between oxygen consumption and carbon dioxide emission is illustrated in Figure 9. Our results highlight the importance of oxygen dynamics and other processes in regulating CO_2 emission from a river-dominated reservoir system.

Conflict of Interest

The authors declared that they have no conflict of interest to this work.

Data Availability Statement

The data presented in this work can be found in the supporting information and can also be accessed at 4TU.Research Data (https://doi.org/10.4121/13838489).

References

Bednarek, A. T. (2001). Undamming rivers: A review of the ecological impacts of dam removal. *Environmental Management*, *27*(6), 803–814. https://doi.org/10.1007/s002670010189

Bennett, E. M., Caraco, N. F., & Carpenter, S. R. (2001). Human impact on erodable phosphorus and eutrophication: A global perspective: Increasing accumulation of phosphorus in soil threatens rivers, lakes, and coastal oceans with eutrophication. *BioScience*, *51*(3), 227–234. https://doi.org/10.1641/0006-3568(2001)051%5B0227:Hioepa%5D2.0.Co;2

Benson, B. B., & Krause, D. (1984). The concentration and isotopic fractionation of oxygen dissolved in freshwater and seawater in equilibrium with the atmosphere. *Limnology & Oceanography*, *29*(3), 620–632. https://doi.org/10.4319/lo.1984.29.3.0620

Bevelhimer, M. S., Stewart, A. J., Fortner, A. M., Phillips, J. R., & Mosher, J. J. (2016). CO_2 is dominant greenhouse gas emitted from six hydropower reservoirs in southeastern United States during peak summer emissions. *Water*, *8*(1), 14. https://doi.org/10.3390/w8010015

Cai, W., Dai, M., Wang, Y., Zhai, W., Huang, T., Chen, S., et al. (2004). The biogeochemistry of inorganic carbon and nutrients in the Pearl River estuary and the adjacent Northern South China Sea. *Continental Shelf Research*, *24*(12), 1301–1319. https://doi.org/10.1016/j.csr.2004.04.005

Carlson, R. E. (1977). A trophic state index for lakes. *Limnology & Oceanography*, *22*(2), 361–369. https://doi.org/10.4319/lo.1977.22.2.0361

Carpenter, S. R., Caraco, N. F., Correll, D. L., Howarth, R. W., Sharpley, A. N., & Smith, V. H. (1998). Nonpoint pollution of surface waters with phosphorus and nitrogen. *Ecological Applications*, *8*(3), 559–568. https://doi.org/10.2307/2641247

Cole, J. J., & Caraco, N. F. (1998). Atmospheric exchange of carbon dioxide in a low-wind oligotrophic lake measured by the addition of SF6. *Limnology & Oceanography*, *43*(4), 647–656. https://doi.org/10.4319/lo.1998.43.4.0647

Crusius, J., & Wanninkhof, R. (2003). Gas transfer velocities measured at low wind speed over a lake. *Limnology & Oceanography*, *48*(3), 1010–1017. https://doi.org/10.4319/lo.2003.48.3.1010

Dai, M., Wang, L., Guo, X., Zhai, W., Li, Q., He, B., & Kao, S.-J. (2008). Nitrification and inorganic nitrogen distribution in a large perturbed river/estuarine system: The Pearl River Estuary, China. *Biogeosciences*, *5*(5), 1227–1244. https://doi.org/10.5194/bg-5-1227-2008

Deemer, B. R., Harrison, J. A., Li, S. Y., Beaulieu, J. J., Delsontro, T., Barros, N., et al. (2016). Greenhouse gas emissions from reservoir water surfaces: A new global synthesis. *BioScience*, *66*(11), 949–964. https://doi.org/10.1093/biosci/biw117

Deemer, B. R., Harrison, J. A., & Whitling, E. W. (2011). Microbial dinitrogen and nitrous oxide production in a small eutrophic reservoir: An in situ approach to quantifying hypolimnetic process rates. *Limnology & Oceanography*, *56*(4), 1189–1199. https://doi.org/10.4319/lo.2011.56.4.1189

Delille, B., Harlay, J., Zondervan, I., Jacquet, S., Chou, L., Wollast, R., et al. (2005). Response of primary production and calcification to changes of pCO$_2$ during experimental blooms of the coccolithophorid Emiliania huxleyi. *Global Biogeochemical Cycles*, *19*(2), 1–14. https://doi.org/10.1029/2004gb002318

Duchemin, E., Lucotte, M., Canuel, R., & Chamberland, A. (1995). Production of the greenhouse gases CH$_4$ and CO$_2$ by hydroelectric reservoirs of the boreal region. *Global Biogeochemical Cycles*, *9*(4), 529–540. https://doi.org/10.1029/95gb02202

Dynesius, M., & Nilsson, C. (1994). Fragmentation and flow regulation of river systems in the Northern third of the world. *Science*, *266*(5186), 753–762. https://doi.org/10.1126/science.266.5186.753

Elser, J. J., Fagan, W. F., Denno, R. F., Dobberfuhl, D. R., Folarin, A., Huberty, A., et al. (2000). Nutritional constraints in terrestrial and freshwater food webs. *Nature*, *408*(6812), 578–580. https://doi.org/10.1038/35046058

Fearnside, P. M. (2001). Environmental impacts of Brazil's Tucurui Dam: Unlearned lessons for hydroelectric development in Amazonia. *Environmental Management*, *27*(3), 377–396. https://doi.org/10.1007/s002670010156

Feray, C., Volat, B., Degrange, V., Clays-Josserand, A., & Montuelle, B. (1999). Assessment of three methods for detection and quantification of nitrite-oxidizing bacteria and Nitrobacter in freshwater sediments (MPN-PCR, MPN-Griess, immunofluorescence). *Microbial Ecology*, *37*(3), 208–217. https://doi.org/10.1007/s002489900144

Fraga, F., Rios, A. F., Perez, F. F., & Figueiras, F. G. (1998). Theoretical limits of oxygen : carbon and oxygen : nitrogen ratios during photosynthesis and mineralisation of organic matter in the sea. *Scientia Marina*, *62*(1–2), 161–168.

Friedl, G., & Wüest, A. (2002). Disrupting biogeochemical cycles—Consequences of damming. *Aquatic Sciences*, *64*(1), 55–65. https://doi.org/10.1007/s00027-002-8054-0

Froelich, P. N. (1980). Analysis of organic carbon in marine sediments. *Limnology & Oceanography*, *25*(3), 564–572. https://doi.org/10.4319/lo.1980.25.3.0564

Giresse, P., Maley, J., & Brenac, P. (1994). Late Quaternary palaeoenvironments in the Lake Barombi Mbo (West Cameroon) deduced from pollen and carbon isotopes of organic matter. *Palaeogeography, Palaeoclimatology, Palaeoecology*, *107*(1–2), 65–78. https://doi.org/10.1016/0031-0182(94)90165-1

Goto, N., Hisamatsu, K., Yoshimizu, C., & Ban, S. (2016). Effectiveness of preservatives and poisons on sediment trap material in freshwater environments. *Limnology*, *17*(1), 87–94. https://doi.org/10.1007/s10201-015-0467-2

Guerin, F., Abril, G., Richard, S., Burban, B., Reynouard, C., Seyler, P., & Delmas, R. (2006). Methane and carbon dioxide emissions from tropical reservoirs: Significance of downstream rivers. *Geophysical Research Letters*, *33*(21), 89–91. https://doi.org/10.1029/2006gl027929

Guérin, F., Abril, G., Serça, D., Delon, C., Richard, S., Delmas, R., et al. (2007). Gas transfer velocities of CO$_2$ and CH$_4$ in a tropical reservoir and its river downstream. *Journal of Marine Systems*, *66*(1), 161–172. https://doi.org/10.1016/j.jmarsys.2006.03.019

Gust, G., & Kozerski, H. P. (2000). In situ sinking-particle flux from collection rates of cylindrical traps. *Marine Ecology Progress Series*, *208*, 93–106. https://doi.org/10.3354/meps208093

Hall, G. H., & Jeffries, C. (1984). The contribution of nitrification in the water column and profundal sediments to the total oxygen deficit of the hypolimnion of a mesotrophic lake (Grasmere, English Lake District). *Microbial Ecology*, *10*(1), 37–46. https://doi.org/10.1007/bf02011593

Hanson, P. C., Bade, D. L., Carpenter, S. R., & Kratz, T. K. (2003). Lake metabolism: Relationships with dissolved organic carbon and phosphorus. *Limnology & Oceanography*, *48*(3), 1112–1119. https://doi.org/10.4319/lo.2003.48.3.1112

Harrison, J. A., Maranger, R. J., Alexander, R. B., Giblin, A. E., Jacinthe, P.-A., Mayorga, E., et al. (2009). The regional and global significance of nitrogen removal in lakes and reservoirs. *Biogeochemistry*, *93*(1–2), 143–157. https://doi.org/10.1007/s10533-008-9272-x

Hayes, N. M., Deemer, B. R., Corman, J. R., Razavi, N. R., & Strock, K. E. (2017). Key differences between lakes and reservoirs modify climate signals: A case for a new conceptual model. *Limnology & Oceanography*, *2*(2), 47–62. https://doi.org/10.1002/lol2.10036

He, B. Y., Dai, M. H., Zhai, W. D., Guo, X. H., & Wang, L. F. (2014). Hypoxia in the upper reaches of the Pearl River Estuary and its maintenance mechanisms: A synthesis based on multiple year observations during 2000-2008. *Marine Chemistry*, *167*, 13–24. https://doi.org/10.1016/j.marchem.2014.07.003

Heiskanen, J. J., Mammarella, I., Haapanala, S., Pumpanen, J., Vesala, T., Macintyre, S., & Ojala, A. (2014). Effects of cooling and internal wave motions on gas transfer coefficients in a boreal lake. *Tellus B: Chemical and Physical Meteorology*, *66*(1), 22827. https://doi.org/10.3402/tellusb.v66.22827

Huang, T. L., Li, X., Rijnaarts, H., Grotenhuis, T., Ma, W. X., Sun, X., & Xu, J. L. (2014). Effects of storm runoff on the thermal regime and water quality of a deep, stratified reservoir in a temperate monsoon zone, in Northwest China. *Science of the Total Environment*, *485–486*, 820–827. https://doi.org/10.1016/j.scitotenv.2014.01.008

Humborg, C., Blomqvist, S., Avsan, E., Bergensund, Y., Smedberg, E., Brink, J., & Mörth, C.-M. (2002). Hydrological alterations with river damming in northern Sweden: Implications for weathering and river biogeochemistry. *Global Biogeochemical Cycles*, *16*(3), 12-1–12-13. https://doi.org/10.1029/2000gb001369

Huttunen, J. T., Väisänen, T. S., Hellsten, S. K., Heikkinen, M., Nykänen, H., Jungner, H., et al. (2002). Fluxes of CH$_4$, CO$_2$, and N$_2$O in hydroelectric reservoirs Lokka and Porttipahta in the northern boreal zone in Finland. *Global Biogeochemical Cycles*, *16*(1), 1–17. https://doi.org/10.1029/2000gb001316

Kumar, A., Yang, T., & Sharma, M. P. (2019a). Greenhouse gas measurement from Chinese freshwater bodies: A review. *Journal of Cleaner Production*, *233*, 368–378. https://doi.org/10.1016/j.jclepro.2019.06.052

Kumar, A., Yang, T., & Sharma, M. P. (2019b). Long-term prediction of greenhouse gas risk to the Chinese hydropower reservoirs. *Science of the Total Environment*, *646*, 300–308. https://doi.org/10.1016/j.scitotenv.2018.07.314

Langdon, C. (2010). *Determination of dissolved oxygen in seawater by Winkler titration using the amperometric technique* (Rep, p. 18). Paris.

Lee, C., Hedges, J. I., Wakeham, S. G., & Zhu, N. (1992). Effectiveness of various treatments in retarding microbial activity in sediment trap material and their effects on the collection of swimmers. *Limnology & Oceanography*, *37*(1), 117–130. https://doi.org/10.4319/lo.1992.37.1.0117

Lewis, E., & Wallace, D. (1998). Program developed for CO$_2$ system calculations. In L. J. Allison (Ed.), *Carbon dioxide information analysis center*. Oak Ridge, TN: Oak Ridge National Laboratory, US Department of Energy.

Li, S. Y., Bush, R. T., Santos, I. R., Zhang, Q. F., Song, K. S., Mao, R., et al. (2018). Large greenhouse gases emissions from China's lakes and reservoirs. *Water Research*, *147*, 13–24. https://doi.org/10.1016/j.watres.2018.09.053

Long, L.-H., Xu, H., Ji, D.-B., Cui, Y.-J., Liu, D.-F., & Song, L.-X. (2016). Characteristic of the water temperature lag in Three Gorges Reservoir and its effect on the water temperature structure of tributaries. *Environmental Earth Sciences*, *75*(22), 1459. https://doi.org/10.1007/s12665-016-6266-1

MacIntyre, S., Romero, J. R., Silsbe, G. M., & Emery, B. M. (2014). Stratification and horizontal exchange in Lake Victoria, East Africa. *Limnology & Oceanography*, *59*(6), 1805–1838. https://doi.org/10.4319/lo.2014.59.6.1805

Mackenthun, A. A., & Stefan, H. G. (1998). Effect of flow velocity on sediment oxygen demand: Experiments. *Journal of Environmental Engineering*, *124*(3), 222–230. https://doi.org/10.1061/(asce)0733-9372(1998)124:3(222)

Matthews, D. A., & Effler, S. W. (2006). Assessment of long-term trends in the oxygen resources of a recovering urban lake, Onondaga Lake, New York. *Lake and Reservoir Management*, *22*(1), 19–32. https://doi.org/10.1080/07438140609353881

McClure, R. P., Hamre, K. D., Niederlehner, B. R., Munger, Z. W., Chen, S. Y., Lofton, M. E., et al. (2018). Metalimnetic oxygen minima alter the vertical profiles of carbon dioxide and methane in a managed freshwater reservoir. *Science of the Total Environment*, *636*, 610–620. https://doi.org/10.1016/j.scitotenv.2018.04.255

Middelburg, J. J. (2019). *Marine carbon biogeochemistry: A primer for Earth system scientists.* Cham, Switzerland: Springer. https://doi.org/10.1007/978-3-030-10822-9

Ministry of Water Resources, P. R. C. (2013). *Bulletin of first national census for water.* Beijing: China Water&Power Press.

Moss, B., Kosten, S., Meerhof, M., Battarbee, R.W., Jeppesen, E., Mazzeo, N., et al. (2011). Allied attack: Climate change and eutrophication. *Inland Waters*, *1*(2), 101–105. https://doi.org/10.5268/IW-1.2.359

Müller, A., & Mathesius, U. (1999). The palaeoenvironments of coastal lagoons in the southern Baltic Sea, I. The application of sedimentary C_{org}/N ratios as source indicators of organic matter. *Palaeogeography, Palaeoclimatology, Palaeoecology*, *145*(1), 1–16. https://doi.org/10.1016/S0031-0182(98)00094-7

Nearing, M., Pruski, F. F., & O'Neal, M. R. (2004). Expected climate change impacts on soil erosion rates: A review. *Journal of Soil and Water Conservation*, *59*(1), 43–50.

Nowlin, W. H., Davies, J.-M., Nordin, R. N., & Mazumder, A. (2004). Effects of water level fluctuation and short-term climate variation on thermal and stratification regimes of a British Columbia Reservoir and Lake. *Lake and Reservoir Management*, *20*(2), 91–109.

Prats, J., Salençon, M.-J., Gant, M., & Danis, P.-A. (2017). Simulation of the hydrodynamic behaviour of a Mediterranean reservoir under different climate change and management scenarios. *Journal of Limnology*, *77*(1), 62–81. https://doi.org/10.4081/jlimnol.2017.1567

Rabalais, N. N., Diaz, R. J., Levin, L. A., Turner, R. E., Gilbert, D., & Zhang, J. (2010). Dynamics and distribution of natural and human-caused hypoxia. *Biogeosciences*, *7*(2), 585–619. https://doi.org/10.5194/bg-7-585-2010

Raymond, P. A., & Cole, J. J. (2001). Gas exchange in rivers and estuaries: Choosing a gas transfer velocity. *Estuaries*, *24*(2), 312. https://doi.org/10.2307/1352954

Redfield, A. C., Ketchum, B. H., & Richards, F. A. (1963). *The influence of organisms on the composition of sea-water* (p. 554).

Rosa, L. P., dos Santos, M. A., Matvienko, B., dos Santos, E. O., & Sikar, E. (2004). Greenhouse gas emissions from hydroelectric reservoirs in tropical regions. *Climatic Change*, *66*(1–2), 9–21. https://doi.org/10.1023/B:CLIM.0000043158.52222.ee

Rosenberg, D. M., McCully, P., & Pringle, C. M. (2000). Global-scale environmental effects of hydrological alterations: Introduction. *BioScience*, *50*(9), 746–751. https://doi.org/10.1641/0006-3568(2000)050%5B0746:gseeoh%5D2.0.co;2

Schwefel, R., Gaudard, A., Wüest, A., & Bouffard, D. (2016). Effects of climate change on deepwater oxygen and winter mixing in a deep lake (Lake Geneva): Comparing observational findings and modeling. *Water Resources Research*, *52*(11), 8811–8826. https://doi.org/10.1002/2016wr019194

Smith, V. H., Tilman, G. D., & Nekola, J. C. (1999). Eutrophication: Impacts of excess nutrient inputs on freshwater, marine, and terrestrial ecosystems. *Environmental Pollution*, *100*(1), 179–196. https://doi.org/10.1016/S0269-7491(99)00091-3

Soumis, N., Duchemin, É., Canuel, R., & Lucotte, M. (2004). Greenhouse gas emissions from reservoirs of the western United States. *Global Biogeochemical Cycles*, *18*(3). https://doi.org/10.1029/2003gb002197

Tranvik, L. J., Downing, J. A., Cotner, J. B., Loiselle, S. A., Striegl, R. G., Ballatore, T. J., et al. (2009). Lakes and reservoirs as regulators of carbon cycling and climate. *Limnology & Oceanography*, *54*(6), 2298–2314. https://doi.org/10.4319/lo.2009.54.6_part_2.2298

Wang, F. S., Wang, B. L., Liu, C. Q., Wang, Y. C., Guan, J., Liu, X. L., & Yu, Y. X. (2011). Carbon dioxide emission from surface water in cascade reservoirs-river system on the Maotiao River, southwest of China. *Atmospheric Environment*, *45*(23), 3827–3834. https://doi.org/10.1016/j.atmosenv.2011.04.014

Wang, S., Yeager, K. M., Wan, G., Liu, C.-Q., Liu, F., & Lu, Y. (2015). Dynamics of CO_2 in a karst catchment in the southwestern plateau, China. *Environmental Earth Sciences*, *73*(5), 2415–2427. https://doi.org/10.1007/s12665-014-3591-0

Wanninkhof, R. (1992). Relationship between wind speed and gas exchange over the ocean. *Journal of Geophysical Research*, *97*(C5), 7373–7382. https://doi.org/10.1029/92jc00188

Weiss, R. F. (1974). Carbon dioxide in water and seawater: The solubility of a non-ideal gas. *Marine Chemistry*, *2*(3), 203–215.

Withers, P. J. A., & Jarvie, H. P. (2008). Delivery and cycling of phosphorus in rivers: A review. *Science of the Total Environment*, *400*(1–3), 379–395. https://doi.org/10.1016/j.scitotenv.2008.08.002

Yu, H., Tsuno, H., Hidaka, T., & Jiao, C. M. (2010). Chemical and thermal stratification in lakes. *Limnology*, *11*(3), 251–257. https://doi.org/10.1007/s10201-010-0310-8

Zavala, C. (2020). Hyperpycnal (over density) flows and deposits. *Journal of Palaeogeography*, *9*(1). https://doi.org/10.1186/s42501-020-00065-x

Zaw, M., & Chiswell, B. (1999). Iron and manganese dynamics in lake water. *Water Research*, *33*(8), 1900–1910. https://doi.org/10.1016/S0043-1354(98)00360-1

Zhai, W. D., Dai, M. H., Cai, W. J., Wang, Y. C., & Wang, Z. H. (2005). High partial pressure of CO_2 and its maintaining mechanism in a subtropical estuary: The Pearl River estuary, China. *Marine Chemistry*, *93*(1), 21–32. https://doi.org/10.1016/j.marchem.2004.07.003

Zhu, X., Gao, A., Lin, J., Jian, X., Yang, Y., Zhang, Y., et al. (2018). Seasonal and spatial variations in rare earth elements and yttrium of dissolved load in the middle, lower reaches and estuary of the Minjiang River, southeastern China. *Journal of Oceanology and Limnology*, *36*(3), 700–716. https://doi.org/10.1007/s00343-018-6207-9

Reference From the Supporting Information

Duchemin, É., Lucotte, M., Canuel, R., Queiroz, A. G., Almeida, D. C., Pereira, H. C., & Dezincourt, J. (2000). Comparison of greenhouse gas emissions from an old tropical reservoir with those from other reservoirs worldwide. *SIL Proceedings, 1922-2010*, *27*(3), 1391–1395.

Li, S., Wang, Y-C., Cao, M., Qian, H.-J., Xu, T., Zhou, Z-R, et al. (2014). Partial pressure and diffusion flux of dissolved carbon dioxide in the mainstream and tributary of the central Three Gorges Reservoir in summer. *Environmental Science*, *35*(03), 885–891.(in Chinese).

Mei, H.-Y, Wang, F.-S., Yao, C.-C, & Wang, B.-I. (2011). Diffusion Flux of partial pressure of dissolved carbon dioxide in Wan-an reservoir in spring. *Environmental Science*, *32*(01), 58–63.(in Chinese).

Peng, X, Liu, C.-Q, Wang, B.-I., Zhago, Y.-C, & Wang, F.-S (2013). Spatial and temporal variation and diffusion flux of surface pCO2 in river-reservoir system. *Earth and Environment*, *41*(02), 97–103.(in Chinese).

Rosa, L. P., Dos Santos, M. A., Matvienko, B., Sikar, E., Lourenço, R. S. M., & Menezes, C. F. (2003). Biogenic gas production from major Amazon reservoirs, Brazil. *Hydrological Processes*, *17*(7), 1443–1450.

Soumis, N., Duchemin, É., Canuel, R., & Lucotte, M. (2004). Greenhouse gas emissions from reservoirs of the western United States. *Global Biogeochemical Cycles*, *18*(3), 367–375.

Wang, S.-I, Wan, G.-J, Liu, C.-Q, Yang, W, Zhu, Z.-Z, Xiao, H.-Y, & Tao, F.-X. (2003). Geochemical changes of CO2 in lakes of Yun-Nan-GuiZhou Plateau and its effect on source and sink of atmospheric CO2. *Quaternary Sciences*, *23*(05), 581–592.(published in Chinese with abstract in English).

Yang, L., Li, H.-P., Sun, B.-F, & Yue, C.-I. (2017). Spatial and temporal variability of CO2 emissions from the Xin'anjiang Reservoir. *Environmental Science*, *38*(12), 5012–5019.(published in Chinese with English abstract).